PCCP

PAPER

View Article Online
View Journal | View Issue

Cite this: *Phys. Chem. Chem. Phys.*, 2017, **19**, 32047

Clarifying the dehydrogenation pathway of catalysed $Li_4(NH_2)_3BH_4$–LiH composites†

G. Amica, *[a] E. C. E. Rönnebro,[b] P. Arneodo Larochette[a] and F. C. Gennari[a]

Received 18th July 2017,
Accepted 15th November 2017

DOI: 10.1039/c7cp04848c

rsc.li/pccp

The effect of different metal oxides (Co_3O_4 and NiO) on the dehydrogenation reaction pathways of the $Li_4(NH_2)_3BH_4$–LiH composite was investigated. The additives were reduced to metallic species *i.e.* Co and Ni which act as catalysts by breaking the B–H bonds in the Li–B–N–H compounds. The onset decomposition temperature was lowered by 32 °C for the Ni-catalysed sample, which released 8.8 wt% hydrogen below 275 °C. It was demonstrated that the decomposition of the doped composite followed a mechanism *via* $LiNH_2$ and Li_3BN_2 formation as the end product with a strong reduction of NH_3 emission. The sample could be partially re-hydrogenated (~1.5 wt%) due to lithium imide/amide transformation. To understand the role of LiH, $Li_4(NH_2)_3BH_4$–LiH–NiO and $Li_4(NH_2)_3BH_4$–NiO composites were compared. The absence of LiH as a reactant forced the system to follow another path, which involved the formation of an intermediate phase of composition $Li_3BN_2H_2$ at the early stages of dehydrogenation and the end products $LiNH_2$ and monoclinic Li_3BN_2. We provided evidence for the interaction between NiO and $LiNH_2$ during heating and proposed that the presence of Li facilitates a NH_x-rich environment and the Ni catalyst mediates the electron transfer to promote NH_x coupling.

1. Introduction

Reversible and safe hydrogen storage systems with a high hydrogen capacity of >10 wt% and propitious sorption kinetics and thermodynamics remain a challenge for the development of onboard vehicle applications.[1,2] Due to the high hydrogen content, much attention has been focused on different combinations of amides and borohydrides.[3–12] On one hand, $LiBH_4$ is a complex hydride known as one of the highest energy density compounds as it contains 18 wt% hydrogen. However, high dehydrogenation temperatures (~500 °C), as well as the evolution of toxic diborane during decomposition, inhibits its utilization as a storage medium.[13] On the other hand, although $LiNH_2$ combined with LiH forms an interesting system which reversibly can store 6.5 wt% hydrogen, the temperatures required for dehydrogenation and rehydrogenation are high for on-board applications.[12]

The synthesis of a new quaternary hydride by mixing $LiNH_2$ and $LiBH_4$ in a 2 : 1 molar ratio, as presented in reaction (1), was first reported in 2005 by Pinkerton *et al.*[14]

$$2LiNH_{2(s)} + LiBH_{4(s)} \rightarrow Li_3BN_2H_{8(s)} \rightarrow Li_3BN_{2(S)} + 4H_{2(g)} \quad (1)$$

This reaction was performed by either ball milling or by heating the mixed powders above 95 °C. They revealed that $Li_3BN_2H_8$ melted at ~190 °C and released 10 wt% hydrogen above ~250 °C with a small amount of ammonia (2–3 mol% of the generated gas), which was distinctly superior to the individual constituents alone under the same conditions. This new compound with the approximate composition of $Li_3BN_2H_8$ could be considered as an appropriate candidate for hydrogen storage applications. Later, *in situ* X-ray diffraction revealed that the single phase $Li_3BN_2H_8$ was in the non-equilibrium state thus decomposing into a $LiNH_2$ enriched α phase with a composition close to $Li_4(NH_2)_3BH_4$ and also a β-phase Li_2BNH_6.[15,16] The main reason for this is that the samples of 2 : 1 ratios that were considered to have good hydrogen sorption properties were actually no longer $Li_3BN_2H_8$ single phase materials. Its true equilibrium state has a body-centered cubic structure $Li_4(NH_2)_3BH_4$ and this is the phase that is worth studying. This compound was synthesized from a 3 : 1 molar ratio as shown in reaction (2) and 8 wt% hydrogen was released by reaction (3):[17]

$$3LiNH_{2(s)} + LiBH_{4(s)} \rightarrow Li_4(NH_2)_3BH_{4(s)} \quad (2)$$

$$Li_4(NH_2)_3BH_{4(s)} \rightarrow Li_3BN_{2(S)} + 1/2Li_2NH_{(S)} + 4H_{2(g)} + 1/2NH_{3(g)} \quad (3)$$

Unfortunately, in this case NH_3 emission was higher (12 mol%) and, as reactions (1) and (3) are exothermic, they are not easily reversible. These materials are also known to be used as lithium fast-ion conductors and have a positive effect on hydrogen uptake

[a] *Consejo Nacional de Investigaciones Científicas y Técnicas, CONICET – Instituto Balseiro (UNCuyo and CNEA), Centro Atómico Bariloche (CNEA), R8402AGP, S. C. de Bariloche, Río Negro, Argentina. E-mail: guillerminaamica@gmail.com*
[b] *Pacific Northwest National Laboratory, 902 Battelle Boulevard, Richland, WA 99352, USA*

† Electronic supplementary information (ESI) available: Fig. S1–S7. See DOI: 10.1039/c7cp04848c

in the Li–Mg–N–H material system. Yang *et al.*[18] presented the idea of a "self-catalyzing" reaction pathway for the $2LiNH_2$–$LiBH_4$–MgH_2 composite and they explained that the enhanced properties resulted from the *in situ* formation of $Li_4(NH_2)_3BH_4$. Cao *et al.*[19] demonstrated that the reaction enthalpy of the $2Mg(NH_2)_2$–3LiH composite was successfully tailored by stabilizing the dehydrogenated product $LiNH_2$ due to the formation of $Li_4(NH_2)_3BH_4$, which was more stable. In our previous work,[20] we studied the $0.7Mg(NH_2)_2$–$1.4LiH$–$0.2Li_4(NH_2)_3BH_4$ composite. We concluded that $Li_4(NH_2)_3BH_4$ has a catalytic role which results in enhanced hydrogen sorption. It was demonstrated that the ionic liquid phase $Li_4(NH_2)_3BH_4$ was involved in the weakening of the N–H bond and, as it melts at a temperature below 200 °C, it provides a liquid medium which improves the mobility of the small ions. Because of the beneficial effects of $Li_4(NH_2)_3BH_4$ in the Li–N–B–H systems, it is interesting to explore it independently. Specifically, there are three problems that need to be solved: (1) the unwanted release of ammonia or diborane, (2) how to decrease the operating temperature and (3) how to obtain reversibility. Thus, strategies such as the use of catalysts, additives and nano-confinement in highly ordered nanoporous carbon have been examined.[21–35]

Zheng *et al.*[21] reported the improved properties of $Li_4(NH_2)_3BH_4$ by adding LiH and Co-catalysts: 9.6 wt% H_2 was released at 250 °C *via* a two-step reaction, which was 100 °C lower compared to the pristine material. The increased mobility of $LiNH_2$ and $LiBH_4$ was due to the formation of melted $Li_4(NH_2)_3BH_4$. It is crucial to highlight that the addition of LiH played a key role in the NH_3 release suppression, which was dramatically reduced from 12 mol% to 0.008 mol%. Previously, Hu *et al.*[22] demonstrated that the NH_3 produced *via* decomposition of $LiNH_2$ could be completely captured by LiH at very short contact times. This ultrafast reaction between NH_3 and LiH inhibits NH_3 formation during the hydrogenation of Li_3N and also prevents hydrogen contamination. In this case, Zheng *et al.*[21] presented the reaction pathway as follows:

$$LiH + Li_4(NH_2)_3BH_4 \rightarrow LiH + LiNH_2 + Li_3BN_2H_8 \quad (4)$$

$$LiH + LiNH_2 \leftrightarrow Li_2NH + H_2 \quad (5)$$

$$Li_3BN_2H_8 \rightarrow Li_3BN_2 + 4H_2 \quad (6)$$

$$\text{In all: } LiH + Li_4(NH_2)_3BH_4 \rightarrow Li_3BN_2 + Li_2NH + 5H_2 \quad (7)$$

The authors concluded that this reaction was not due to a fast combination of LiH and NH_3. However, they did not observe the formation of $Li_3BN_2H_8$, which is not a stable compound. Later, Zhang *et al.*[23] introduced CoO into the Li–B–N–H system as a catalyst precursor. They studied the dehydrogenation behavior of the $LiBH_4$–$2LiNH_2$–xCoO (x = 0–0.2) composites and observed that decomposition occurred simultaneously with the melting of $Li_4(NH_2)_3BH_4$. The onset dehydrogenation temperature decreased to 120 °C for the sample with the addition of 0.05 CoO. This composition showed 30% reduction in the activation energy. They concluded that metallic Co from the reduction of CoO acted as the catalytic active species. It is interesting to point out that this sample was partially recharged (1.1 wt% at 350 °C with 110 atm hydrogen pressure). Later, they proved that by adding a minor quantity of CoO to the $LiBH_4{\cdot}NH_3$–3LiH system, the dehydrogenation temperature was reduced to 90 °C.[28] The metallic Co and the formed Co – B species were well dispersed and acted as active catalysts breaking the B–H bonds of the Li–B–N–H species. A similar effect[24] has been observed with the addition of a small amount of Co_3O_4 to the $LiBH_4$–$2LiNH_2$ system but, in this case, 1.7 wt% hydrogen was absorbed under a hydrogen pressure of 110 bar at 220 °C. Moreover, the addition of nano-sized particles such as Ni[25–27] allowed the formation of Ni-containing compounds that were found to have a remarkable catalytic activity by reducing kinetic barriers of hydrogen release, which resulted in lowering of the operating temperatures. Li *et al.*[25] showed that Ni particles reacted with $LiBH_4$ to form *in situ* Ni_4B_3 and that Ni_2B was produced after rehydrogenation. They proved that both species catalysed the dehydrogenation of unreacted $LiBH_4$. The activation energy of dehydrogenation was reduced from 187 ± 24 kJ mol^{-1} to 100 ± 4 kJ mol^{-1}.

Motivated by previous research which showed how the addition of certain catalysts and LiH reduced its decomposition temperature and the amount of evolved NH_3, we studied the effect of adding different oxides to the $Li_4(NH_2)_3BH_4$–LiH composite with the aim to facilitate decomposition. Specifically, a comparative study of the hydrogen storage properties of this composite with and without 5 wt% NiO and Co_3O_4 was performed using the same experimental conditions. The purpose of this work is to clarify the effect of the different metal oxides and the role of LiH on the kinetics of the Li–B–N–H system and hence, the chemical interactions and the dehydrogenation reaction pathways.

2. Experimental

2.1 Synthesis of the composites

The $Li_4(NH_2)_3BH_4$–LiH composite was prepared using the commercial materials $LiNH_2$ (Aldrich, 95%), $LiBH_4$ (Aldrich, 90%), and LiH (Fluka, 95%) in a molar ratio of 3 : 1 : 1. To study the effect of different additives on the pristine material, the following mixtures were also considered: $Li_4(NH_2)_3BH_4$–LiH–5 wt% X (X: Co_2O_3, NiO) and $Li_4(NH_2)_3BH_4$–5 wt% NiO. The materials were handled in a MBraun Unilab argon-filled glove box, with oxygen and moisture levels lower than 5 ppm due to their high reactivity. For all studies, high purity hydrogen (Linde, 99.999%) and argon (Linde, 99.999%) were used. All samples were milled for 5 hours in a planetary ball mill (Fritsch Pulverisette 6) at 500 rpm with a ball to powder mass ratio of 53 : 1, using a sequence of 15 min milling and 10 min pause. Possible unreacted zones were eliminated by mixing the material after 1 h and 3 h of milling using mortar and pestle in the glove box.

2.2 Characterization of the composites

The structural, thermal and hydrogen storage properties of the as-milled and as-cycled samples were studied using differential scanning calorimetry (DSC, TA 2910 calorimeter), X-ray powder diffraction (PXRD, PANalytical Empyrean), Fourier transform

infrared spectroscopy (FTIR, Perkin Elmer Spectrum 400 with MCT detector), thermogravimetry (TG-HP50, TA Instruments), NMR and Sieverts type apparatus. Structural information of the samples was obtained by PXRD (Cu Kα radiation, graphite monochromator) and FTIR analyses. During the PXRD data collection, an airtight holder was employed to prevent the reaction between samples and air. For IR spectroscopy measurements, the samples were mixed with dry KBr under a purified argon atmosphere, pressed to pellets and placed in a specially designed airtight cell. For the $Li_4(NH_2)_3BH_4$–LiH–NiO and $Li_4(NH_2)_3BH_4$–NiO composites, the gases released at different temperatures (100, 150, 200, 250 and 350 °C) were collected in a degassed quartz optical cell with KBr windows and the gas phase spectra were taken at room temperature. The thermal behavior of the samples was studied by DSC with a heating ramp of 5 °C min^{-1} and an argon flow rate of 122 ml min^{-1}. Non-isothermal dehydrogenations were carried out using modified Sieverts type equipment, coupled with a mass flow controller from room temperature up to 400 °C against 0.5 bar (50 kPa) back pressure. The $Li_4(NH_2)_3BH_4$–LiH–NiO and $Li_4(NH_2)_3BH_4$–NiO composites were measured and each one was stopped at variable hydrogen content (points: (1) as-milled, (2) 1 wt%, (3) 5 wt% and (4) completely decomposed) to determine the crystalline phases. Rehydrogenation was performed at 200 °C under 60 bar (6.0 MPa) for 20 hours. Morphological observations were carried out using SEM-FEI-Nova Nano SEM 230. Three of the $Li_4(NH_2)_3BH_4$–LiH–NiO obtained samples (1, 2 and 4) were investigated by ^{11}B Magic angle spinning Nuclear Magnetic Resonance (MAS NMR). The NMR samples were packed into boron-free zirconia rotors under an inert atmosphere. The sample was referenced to $NaBH_4$ (−41 ppm), and experiments were performed at 7.1 T, 300 MHz and ^1H frequency at room temperature.

3. Results and discussion

3.1 Dehydrogenation properties of the samples

Non-isothermal measurements were carried out from room temperature up to 400 °C to investigate the dehydrogenation properties of $Li_4(NH_2)_3BH_4$ when using different additives. The starting temperature was considered to be the temperature at which 5% of the reactants have converted. From volumetric measurements, the $Li_4(NH_2)_3BH_4$–LiH composite started reacting at 243 °C and the reaction completed at 350 °C (Fig. 1A). Approximately 11.3 wt% hydrogen was released with a one-step reaction. The dehydrogenation onset temperature was decreased to 14 °C for the Co-catalysed sample. The destabilizing effect of the NiO addition was better defined and the composite decomposition started at 221 °C, which is 32 °C lower than that of the pristine sample. The $Li_4(NH_2)_3BH_4$–LiH–NiO composite could release 8.8 wt% of its hydrogen below 275 °C. When the temperature was higher than 275 °C decomposition was significantly decelerated and between 275 and 350 °C it released an additional 1.8 wt%. TG measurements were in agreement with non-isothermal observations as can be seen in Fig. 1B. All the samples that contained LiH showed similarity in the capacity, which suggested that mostly hydrogen was released

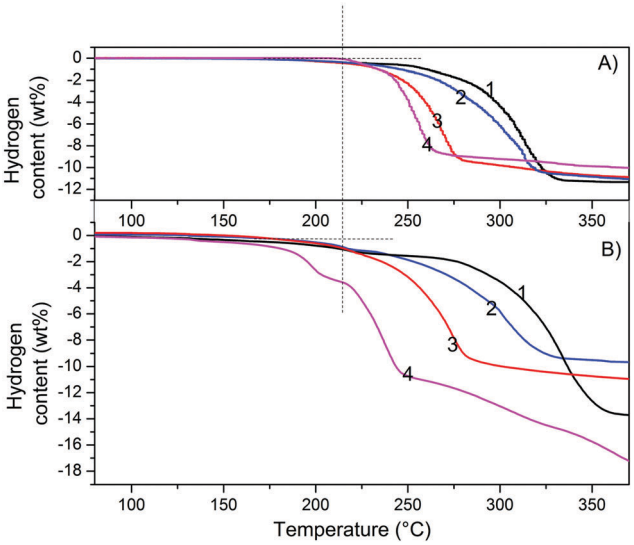

Fig. 1 Non-isothermal measurements (A) volumetric technique and (B) TG curves of samples $Li_4(NH_2)_3BH_4$–LiH (1), $Li_4(NH_2)_3BH_4$–LiH –Co_2O_3 (2), $Li_4(NH_2)_3BH_4$–LiH–NiO (3) and $Li_4(NH_2)_3BH_4$–NiO (4).

and the differences could be justified within the intrinsic error. Discrepancies between the storage capacities of volumetric and TG measurements arise from the uncertainties introduced in the determination of the small mass TG samples (about 10%). However, TG and volumetric curves of the $Li_4(NH_2)_3BH_4$–NiO sample presented some differences in the shape, especially at the first-stage of dehydrogenation. In fact, decomposition of $Li_4(NH_2)_3BH_4$ began at lower temperature which might be related to the absence of LiH and the catalytic effect of Ni. Then, it is interesting to point out that the effect of NH_3 suppression by the addition of LiH was evident.

Gas FTIR analysis was performed for the $Li_4(NH_2)_3BH_4$–LiH (see Fig. S1, ESI†), $Li_4(NH_2)_3BH_4$–LiH–NiO and $Li_4(NH_2)_3BH_4$–NiO samples (Fig. 2) to study the gases released under annealing. Using this technique it could be determined that for the $Li_4(NH_2)_3BH_4$–LiH–NiO sample, most of the gas released up to 250 °C was hydrogen and no NH_3 emission was detected below 350 °C. A small amount of methane was detected at 200 and 250 °C, which is due to residual contamination in the as-received $LiNH_2$. The emission of water and/or diborane was ruled out. This result was in agreement with the non-isothermal and thermogravimetric measurements (Fig. 1). On the other hand, for the $Li_4(NH_2)_3BH_4$–NiO sample, a significant amount of NH_3 was detected at 100 °C, *i.e.* 0.4 mol%, and the emission increased with temperature. The large amount of NH_3, which is released simultaneously with hydrogen while heating, inhibits its utilization as a storage material. The difference observed for these two samples was attributed to the role of LiH. This is supported by the decomposition of pristine $Li_4(NH_2)_3BH_4$ which starts to release NH_3 near its melting point.[21] In the case of the $Li_4(NH_2)_3BH_4$–LiH sample, methane was detected at 200, 250 and 350 °C (Fig. S1, ESI†). Moreover, at 200 °C, an incipient release of NH_3 was observed and the amount increased as the temperature increased. Then, the promoted NH_3 emission for

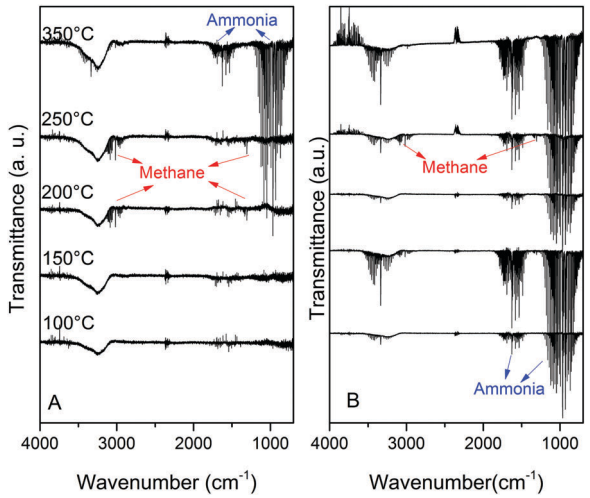

Fig. 2 FTIR gas spectra for samples $Li_4(NH_2)_3BH_4$–LiH–NiO (A) and $Li_4(NH_2)_3BH_4$–NiO (B).

$Li_4(NH_2)_3BH_4$–NiO relative to the pristine material could be associated with the role of Ni as the catalyst. It should be highlighted that no NH_3 release was detected for the $Li_4(NH_2)_3BH_4$–LiH–NiO sample at 200 °C.

The DSC profiles for all the samples are shown in Fig. 3. The curve for the pristine sample presents a double endothermic peak at 216 and 220 °C due to the $Li_4(NH_2)_3BH_4$ melting and due to the H_2 release respectively; this shape was already seen by Zheng *et al.*[21]

Moreover, two small endothermic peaks are overlapping with a wide exothermic one around 330 °C attributed to the $Li_4(NH_2)_3BH_4$ dissociation. In the case of the Co_2O_3 and NiO doped composites, the main difference is the existence of a flat base line for temperatures over 275 °C, which indicates that NH_3 emission was reduced and/or eliminated (see Fig. 2). Furthermore, the absence of an endothermic peak at 134 °C in all curves which would correspond to the melting point of Li_2BNH_6[28] indicates that this phase was not produced as a consequence of heating. Here the starting material was in $3LiNH_2$:$1LiBH_4$ proportion; the absence of Li_2BNH_6 is consistent with the result

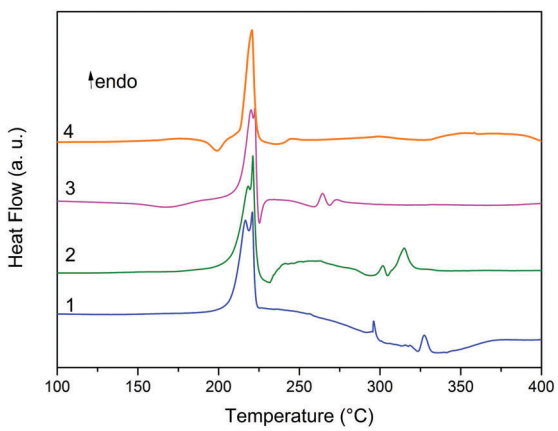

Fig. 3 DSC profiles for samples $Li_4(NH_2)_3BH_4$–LiH (1), $Li_4(NH_2)_3BH_4$–LiH–Co_2O_3 (2), $Li_4(NH_2)_3BH_4$–LiH–NiO (3) and $Li_4(NH_2)_3BH_4$–NiO (4).

of previous reports.[16] The phase diagram presented by Meisner *et al.*[16] indicates that in the rich zone of $LiNH_2$, a mixture of α phase and $LiNH_2$ should be expected. In the case of the $Li_4(NH_2)_3BH_4$–NiO sample, there was an exothermic event at 200 °C which is related to the interaction between the additive and $Li_4(NH_2)_3BH_4$. The main endothermic peak was at the same position. Independently of the additive, the splitting of the main peak into two peaks implies that there is a common mechanism for the samples with LiH. On the other hand, since the sample without LiH showed a single principal peak instead, a difference in the reaction mechanism should be considered. The same observation was achieved through TG and volumetric measurements.

Structural characterization of the as-milled and completely decomposed samples was carried out by powder X-ray diffraction (PXRD) (Fig. S2, ESI†). For the pristine sample, the $Li_4(NH_2)_3BH_4$ compound and LiH were identified, as well as an excess of $LiNH_2$. This indicates that there was a chemical reaction between $LiNH_2$ and $LiBH_4$ during ball milling to produce a quaternary Li–B–N–H phase. Previous studies have pointed out that the extra $LiNH_2$ merges into the $Li_4(NH_2)_3BH_4$ structure when heating.[17,21] Moreover, the single phase 2 : 1 $Li_3BN_2H_8$ was not expected to be found because *in situ* PXRD experiments have previously clarified that this phase changes with time into a combination of a $LiNH_2$ enriched α phase and the 1 : 1 β phase Li_2BNH_6. On the other hand, the decomposed sample was a mixture of Li_3BN_2 (both tetrahedral and monoclinic structures), Li_2NH and Li_2O. With respect to the doped samples after ball milling; the compound $Li_4(NH_2)_3BH_4$ was formed together with a little $LiNH_2$ in excess in all cases. No weakening of the main phase $Li_4(NH_2)_3BH_4$ was observed with the incorporation of the additives. The species Co_3O_4/CoO and NiO were clearly identified in each case, demonstrating that they did not interact either with $LiNH_2$, LiH or $LiBH_4$ and remained unmodified during milling. The decomposed states included Li_3BN_2 (tetrahedral and monoclinic structures) and Li_2NH in all the doped samples. Moreover, all of them presented Li_2O. Metallic Co and Ni were also identified for the Co_2O_3 and NiO doped composite respectively. It is expected that the *in situ* formed Co and Ni, due to reduction of the oxides, act as catalysts by breaking the B–H bonds of the Li–B–N–H species and promoting the dehydrogenation process.[32,33] In summary, the phases after mechanical milling and in the decomposed state are presented in Table 1. In the samples $Li_4(NH_2)_3BH_4$–LiH–Co_2O_3 and $Li_4(NH_2)_3BH_4$–LiH–NiO, the CoO–Co_3O_4 and NiO additives were reduced to metallic Co and Ni respectively. The distribution of Co and Ni was observed by scanning electron microscopy (SEM) using backscattered electrons (Fig. S3, ESI†). The images did not confirm that the differences in the sorption behavior were due to the metal oxide particle size or its distribution because they seem to be quite similar. In addition, the agglomerate size distribution of the composite remains similar independently of the catalyst nature. The sample with NiO contained a higher amount of metallic atoms than the sample with Co_2O_3, which could favor the catalytic activity of Ni. However, this difference was small and the decomposition behavior was much better for

Table 1 Phases present in the $Li_4(NH_2)_3BH_4$–LiH, $Li_4(NH_2)_3BH_4$–LiH–Co_2O_3 and $Li_4(NH_2)_3BH_4$–LiH–NiO samples after mechanical milling and after complete decomposition

Sample	Mechanical milling	Complete decomposition
$Li_4(NH_2)_3BH_4$–LiH	$Li_4(NH_2)_3BH_4$ LiH $LiNH_2$	Li_3BN_2 Li_2NH Li_2O
$Li_4(NH_2)_3BH_4$–LiH–Co_2O_3	$Li_4(NH_2)_3BH_4$ $LiNH_2$ Co_3O_4/CoO	Li_3BN_2 Li_2O Li_2NH Co
$Li_4(NH_2)_3BH_4$–LiH–NiO	$Li_4(NH_2)_3BH_4$ LiH $LiNH_2$ NiO	Li_3BN_2 Li_2NH Li_2O Ni

the Ni-doped sample. Then, further analysis of the $Li_4(NH_2)_3BH_4$–LiH–NiO sample will be presented in the following sections.

3.2 Structural characterization of $Li_4(NH_2)_3BH_4$–LiH–NiO and $Li_4(NH_2)_3BH_4$–NiO at different stages of decomposition

In order to understand the reaction pathway for the hydrogen release of the $Li_4(NH_2)_3BH_4$–LiH–NiO and $Li_4(NH_2)_3BH_4$–NiO samples, the phases in the different states of this process were determined using PXRD and FTIR. Non-isothermal measurements were stopped at selected temperatures that correspond to different hydrogen contents, referred to as: (1) as-milled, (2) 1 wt%, (3) 5 wt% and (4) 10.6 wt% (fully decomposed). Fig. 4 and 5 show the PXRD and FTIR profiles for the sample $Li_4(NH_2)_3BH_4$–LiH–NiO. As previously mentioned, after ball milling this sample was mostly $Li_4(NH_2)_3BH_4$. $LiNH_2$ and LiH were also clearly identified. The 2θ positions 37.24°, 43.28°, 62.85° and 75.39° were attributed unequivocally to NiO. $Li_4(NH_2)_3BH_4$ formation was identified by its characteristic N–H vibrations at 3301 and 3243 cm^{-1}, as well as residual $LiNH_2$ by its characteristic bands at 3313, 3258 and 1540 cm^{-1}. Moreover, FTIR analysis shows the peaks of the B–H vibrations of the BH_4 group at 2387, 2293 and 2225 cm^{-1} and also at 1271, 1221, 1126

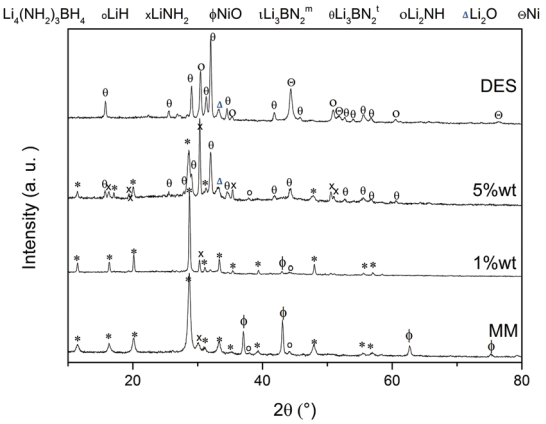

Fig. 4 Powder X-ray diffraction of the $Li_4(NH_2)_3BH_4$–LiH–NiO sample at different stages of dehydrogenation.

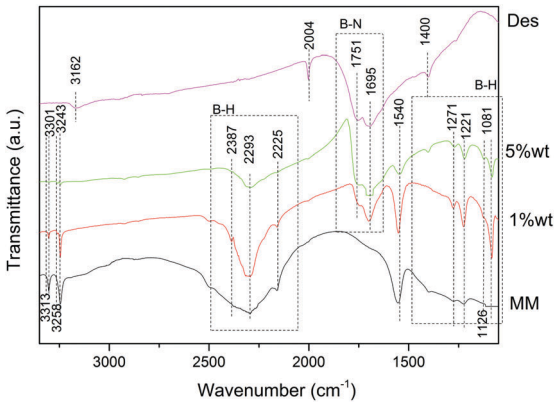

Fig. 5 FTIR of the $Li_4(NH_2)_3BH_4$–LiH–NiO sample at different stages of dehydrogenation.

and 1081 cm^{-1}.[24,28,34] After 1 wt% hydrogen release the PXRD pattern was unchanged, but in this case only the most intense peak of NiO at 43.28° was recognizable. In addition to the N–H and B–H vibrations[34] of the NH_2 and BH_4 groups corresponding to $Li_4(NH_2)_3BH_4$, two new bands at 1751 and 1695 cm^{-1} were assigned to the B–N vibrations, which indicate the incipient formation of the tetragonal Li_3BN_2 phase.[24,28]

After 5 wt% hydrogen release, the PXRD changed substantially. $Li_4(NH_2)_3BH_4$ and LiH could still be recognized but the intensity of the peaks of the tetrahedral dehydrogenated product Li_3BN_2 increased. Moreover, the peaks related to $LiNH_2$ became sharper, indicating that the amount of $LiNH_2$ increased. FTIR analysis was consistent with those observations. Li_2O was also unambiguously identified from its diffraction peak at 32.78°. No species containing Ni were identified, which means that the Ni compound either became amorphous or reacted to form another amorphous phase. Finally, after complete decomposition of the sample releasing 10.6 wt% hydrogen, the diffraction patterns of both tetrahedral and monoclinic Li_3BN_2 were observed, Li_2NH was visible and Li_2O was still present. Either NiO or LiH was identified but instead metallic Ni was identified from its diffraction positions at 2θ = 44.68° and 42.7°. FTIR analysis clearly revealed the absence of $LiNH_2$ and Li_2NH, which was unequivocally recognized for its characteristic band at 3162 cm^{-1}. No B–H vibrations corresponding to the $[BH_4]^-$ group were identified, which implies that $Li_4(NH_2)_3BH_4$ was completely decomposed.

Characterization of the $Li_4(NH_2)_3BH_4$–LiH–NiO sample was also performed by ^{11}B solid state MAS NMR, which provides information about the chemical environments of B for the sample at different stages of dehydrogenation (see Fig. S4, ESI†). For the ball milled sample, a chemical shift of −39.81 ppm for B in $[BH_4]$ was observed. B in the phase $Li_4(NH_2)_3BH_4$ is more electron rich than B in $LiBH_4$ which has a chemical shift of −41.62 ppm.[35] We did not identify phases of different stoichiometries such as Li_2BNH_6 which for example would have a chemical shift of −37.88 ppm or $Li_3BN_2H_8$. The spectra of the 1 wt% decomposed sample exhibited the same shape. As dehydrogenation progressed, the chemical environment of B changed from $[BH_4]$ to $[BN_2]$. For the fully dehydrogenated

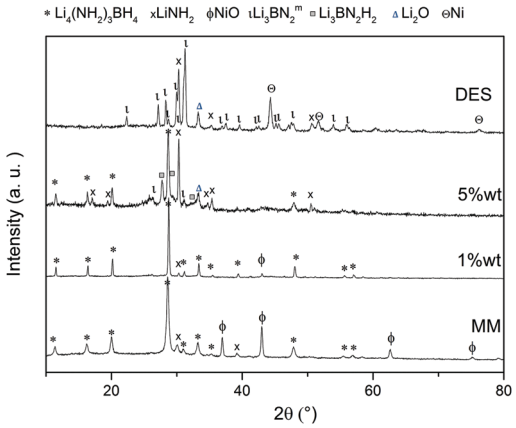

Fig. 6 Powder X-ray diffraction of the $Li_4(NH_2)_3BH_4$–NiO sample at different stages of dehydrogenation.

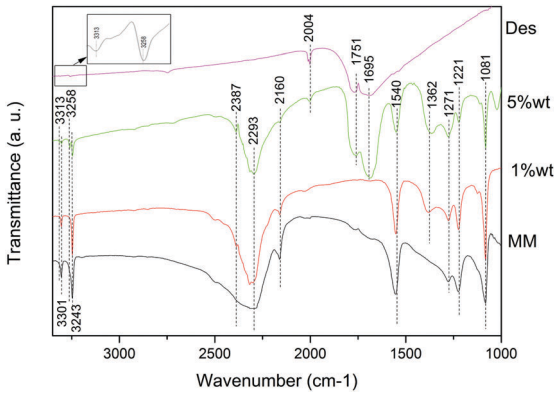

Fig. 7 FTIR of the $Li_4(NH_2)_3BH_4$–NiO sample at different stages of dehydrogenation.

sample the spectra show a broad signal covering the range between 3 and 30 ppm. There was no evidence for the formation of nickel borides.[36]

After ball milling the $Li_4(NH_2)_3BH_4$–NiO sample consisted mainly of $Li_4(NH_2)_3BH_4$, $LiNH_2$ and NiO as expected (see Fig. 6). The FTIR bands characterized by the N–H vibrations associated with $Li_4(NH_2)_3BH_4$ (3301, 3243 cm^{-1}) and $LiNH_2$ (3313, 3258 and 1540 cm^{-1}) were observed (see Fig. 7). In this case the B–H vibrations in the region between 2380 and 2160 cm^{-1} and 1400 and 1000 cm^{-1} were also identified.[24,28,32] As for the $Li_4(NH_2)_3BH_4$–LiH–NiO sample, after releasing 1 wt% hydrogen, the sample does not change much; $Li_4(NH_2)_3BH_4$ was still observed as well as $LiNH_2$. Moreover, the most intense peak of NiO could be recognized. As the process continued, after the release of 5 wt% hydrogen, the diffraction peak at 32.8° was attributed to Li_2O in addition to the previously mentioned phases. In contrast to the sample $Li_4(NH_2)_3BH_4$–LiH–NiO, only the monoclinic structure of the Li_3BN_2 phase appeared. Simultaneously, three peaks at positions 28.0, 29.3 and 32.1° were associated with an intermediate phase of composition $Li_3BN_2H_2$, which has been previously reported by Pinkerton *et al.*[17] The band at 1362 cm^{-1} is also related to this intermediate phase and it is also seen in the 1 wt% sample (Fig. 6). The characteristic bands of the B–N bonds (1751 and 1695 cm^{-1}) were identified by FTIR (Fig. 7). Finally, in the fully decomposed state monoclinic Li_3BN_2 and Li_2O were observed. $LiNH_2$ was not completely decomposed. Its presence was unequivocally demonstrated by the identification of its characteristics bands at 3313 and 3258 cm^{-1} by FTIR and in addition, the absence of Li_2NH could be assured as no band at 3160 cm^{-1} was observed. As for the $Li_4(NH_2)_3BH_4$–LiH–NiO sample, NiO was reduced to metallic Ni.

In summary, the phases at different stages of dehydrogenation for both samples are presented in Table 2.

3.3 Dehydrogenation pathway for the $Li_4(NH_2)_3BH_4$–LiH–NiO and $Li_4(NH_2)_3BH_4$–NiO samples

3.3.1 Dehydrogenation pathway for the $Li_4(NH_2)_3BH_4$–LiH–NiO sample. On the basis of the analysis results obtained by a combination of FTIR and PXRD techniques (Table 2), the following reaction was expected to take place during dehydrogenation:

$$Li_4(NH_2)_3BH_4 + LiH \rightarrow Li_3BN_2 + LiNH_2 + 4H_2 + LiH \quad (8)$$

$Li_4(NH_2)_3BH_4$ was recognized at different stages of the reaction, which means that this phase gradually changed its composition as the process advanced, becoming less rich in $LiNH_2$. The occurrence of reaction (8) was also confirmed by the detection of Li_3BN_2 at 1 wt% as a consequence of the $Li_4(NH_2)_3BH_4$ decomposition and by the increased amount of $LiNH_2$ after about 50% of decomposition has been completed. Considering only this equation and calculations with respect to the total mass of the mixture, the theoretical capacity is 8.1 wt%, which is lower than the wt% obtained from non-isothermal volumetric and thermogravimetric measurements and suggests that there is another source of hydrogen.

PXRD analysis confirmed that in the decomposed state there were no remains of $Li_4(NH_2)_3BH_4$ and $LiNH_2$. For that reason, we can assure that reaction (8) occurred in the initial stage and then, at later stages of dehydrogenation, lithium imide was formed from the reaction of lithium amide with LiH:

$$LiNH_2 + LiH \rightarrow Li_2NH + H_2 \quad (9)$$

$$\text{In total: } Li_4(NH_2)_3BH_4 + LiH \rightarrow Li_3BN_2 + Li_2NH + 5H_2 \quad (10)$$

Carrying out the calculations analogously, the decomposition of this amide in the presence of LiH provides an extra hydrogen capacity of 2.0 wt%. Furthermore, there was evidence for the disappearance of Ni simultaneously with the formation of Li_2O, then, the reaction between NiO and LiH should be considered:[21,37]

$$NiO + 2LiH \rightarrow Ni + Li_2O + H_2 \quad \Delta G^0\ (200\ ^\circ C) = -234\ kJ\ mol^{-1} \quad (11)$$

In fact, Ni is detected as a crystalline phase at the end of dehydrogenation. As the amount of additive was small, through this reaction only 0.13 wt% hydrogen was released.

Finally, bearing in mind that LiH is consumed, the capacity of reaction (9) turns out to be 1.75 wt%. Then, after adding

Table 2 Phases present in the $Li_4(NH_2)_3BH_4$–LiH–NiO and $Li_4(NH_2)_3BH_4$–NiO samples at different stages of dehydrogenation

	$Li_4(NH_2)_3BH_4$–LiH–NiO		$Li_4(NH_2)_3BH_4$–NiO	
Stage	PXRD	FTIR	PXRD	FTIR
MM	$Li_4(NH_2)_3BH_4$ $LiNH_2$ LiH NiO	$Li_4(NH_2)_3BH_4$ $LiNH_2$	$Li_4(NH_2)_3BH_4$ $LiNH_2$ NiO	$Li_4(NH_2)_3BH_4$ $LiNH_2$
1 wt%	$Li_4(NH_2)_3BH_4$ $LiNH_2$ LiH NiO	$Li_4(NH_2)_3BH_4$ $LiNH_2$ Li_3BN_2	$Li_4(NH_2)_3BH_4$ $LiNH_2$ NiO	$Li_4(NH_2)_3BH_4$ $LiNH_2$ $Li_3BN_2H_2$
5 wt%	$Li_4(NH_2)_3BH_4$ $LiNH_2$ Li_2O Li_3BN_2 (T)	$Li_4(NH_2)_3BH_4$ $LiNH_2$ Li_3BN_2	$Li_4(NH_2)_3BH_4$ $LiNH_2$ Li_3BN_2 (M) Li_2O $Li_3BN_2H_2$	$Li_4(NH_2)_3BH_4$ $LiNH_2$ Li_3BN_2 $Li_3BN_2H_2$
Decomposed state	Li_3BN_2 (T + M) Li_2NH Li_2O Ni	Li_2NH Li_3BN_2	Li_3BN_2 (M) $LiNH_2$ Li_2O Ni	$LiNH_2$ Li_3BN_2

hydrogen in reactions (8), (9) and (11) the total capacity of the $Li_4(NH_2)_3BH_4$–LiH–NiO sample was approximately 9.6 wt%.

This value was still smaller than the one obtained *via* non-isothermal measurements, *i.e.* 10.6 and 10.7 wt% by volumetric and thermogravimetric measurements, respectively. The difference between these calculations and the TG results could be attributed to the ammonia emission, which turns out to be about 0.06 mol% NH_3. This amount is comparable to previous studies.[24] Finally, the experimental evidence shows that the dehydrogenation pathway of the $Li_4(NH_2)_3BH_4$–LiH composite occurs *via* $LiNH_2$ and Li_3BN_2 formation. As the reaction progresses, the $Li_4(NH_2)_3BH_4$ phase remains instead of $Li_3(NH_2)_2BH_4$, as was previously proposed.[21] Then, the $Li_4(NH_2)_3BH_4$–LiH composite can be considered as a destabilized composite that releases hydrogen near the melting point of $Li_4(NH_2)_3BH_4$ with a strong reduction of NH_3 emission. As was suggested by Zheng *et al.*, the dehydrogenation of $Li_4(NH_2)_3BH_4$–LiH does not seem to be an ammonia mediated mechanism.[21] In fact, a direct solid–solid reaction mechanism between $Li_4(NH_2)_3BH_4$ and LiH could be favored when mixing is good and efficient.[38] We propose that near the melting point of $Li_4(NH_2)_3BH_4$, its structure is destabilized and the mobility of $LiNH_2$ and $LiBH_4$ increased, while LiH is in the neighborhood. Then, hydrogen release is possible due to the simultaneous combination of H^+ from NH_2 groups and H^- from the BH_4 group and LiH. In fact, after 1 wt% hydrogen was released, Li_3BN_2 was identified (Fig. 6), which indicates the collapse of $Li_4(NH_2)_3BH_4$ while no NH_3 emission was detected (Fig. 2).

The main role of Ni is to catalyze the dehydrogenation of $Li_4(NH_2)_3BH_4$ by activation of the B–H bond at this temperature,[32,33] decreasing the temperature and improving the rate of dehydrogenation. Similar results were observed in previous studies using Co and Ni oxides and/or chlorides.[21,24,27,28,31] Note that after 1 wt% of dehydrogenation and because of its poor crystallinity, Ni was difficult to identify. Crystalline Ni was detected only after heating to high temperatures.

In order to investigate the reversibility of the $Li_4(NH_2)_3BH_4$–LiH composite, the decomposed $Li_4(NH_2)_3BH_4$–LiH–NiO sample was exposed to 60 bar (6000 kPa) at 220 °C for 20 h. The sample was partially re-hydrogenated: 1.5 wt% hydrogen was released in the second dehydrogenation (Fig. S5, ESI†). This value is similar to the calculated amount (~1.65 wt%).

The presence of lithium amide indicates that the reversibility is mainly due to the rehydrogenation of lithium imide and that Li_3BN_2 could not be rehydrogenated under these conditions.

3.3.2 Dehydrogenation pathway for the $Li_4(NH_2)_3BH_4$–NiO sample. At this point, in previous sections we have demonstrated that there is a similar mechanism for the samples that contain LiH and that the absence of LiH as a reactant forces the system to follow another path. As a starting point, the work performed by Pinkerton *et al.*, in which the dehydrogenation behavior of nickel-chloride-catalysed stoichiometric $Li_4(NH_2)_3BH_4$ was studied,[17] must be taken into consideration. In these investigations, LiH was not employed in the initial mixtures. They worked on determining whether hydrogen and ammonia were cogenerated from a single decomposition reaction or whether they evolved in two distinct decomposition reactions that occur at about the same temperature. They demonstrated that the two gases were evolved in two distinct decomposition reactions that are coincident in un-catalysed $Li_4(NH_2)_3BH_4$, but can be separated by a dehydrogenation catalyst. The main difference between this work and the experiments of Pinkerton *et al.* is as follows: in order to remove the ammonia effect from decomposition at low temperatures, they performed a preliminary heat treatment limited to a temperature high enough (higher than 140 °C) to achieve full NH_3 release while limiting the amount of lost H_2. In our case, we considered that it was important to take into account the ammonia released from the early steps of the reaction. *In situ* FTIR gas analysis showed ammonia release at low temperatures. This is not due to $LiNH_2$ decomposition because at low temperatures its rate is very low. Pinkerton *et al.* proposed that NH_3 could appear as a consequence of the

accommodation of $LiNH_2$ into the α-phase during heating. It could also be the situation for NiO catalysed $Li_4(NH_2)_3BH_4$, where NH_3 was detected at 150 °C. However, decompositions at higher temperatures generate additional emissions of H_2 and NH_3. To come up with the reaction pathway, it is important to keep in mind that catalysed $Li_4(NH_2)_3BH_4$ presented two interesting issues. First, an intermediate phase of composition $Li_3BN_2H_2$ was identified by PXRD during dehydrogenation.[17,28] This phase was formed during the early stage of decomposition and thus helps in understanding the first stage of the reaction pathway. In fact, the amount of intermediate phase, as well as of $LiNH_2$, increases the hydrogen release from 1 wt% to 5 wt% (see Fig. 6). Then, at this stage dehydrogenation can be expressed by reaction (12) which accounts for 6.6 wt% hydrogen.

$$Li_4(NH_2)_3BH_4 \rightarrow Li_3BN_2H_2 + LiNH_2 + 3H_2 \quad (12)$$

Secondly, in a completely decomposed state, only the monoclinic structure of Li_3BN_2 was detected. In fact, to assure that Li_3BN_2 only crystallized in this structure and not in the tetrahedral structure, similar decomposition was performed but stopped barely in time and temperature. In this case, Li_3BN_2 seemed not to be completely crystalline yet and some small peaks of the monoclinic structure were recognized, as well as $LiNH_2$, Li_2O and incipient Ni (see Fig. S6, ESI†). Simultaneously, the intermediate phase remains. This means that the existence of the monoclinic structure was not a consequence of exposing the decomposed sample to a longer period under temperature treatment to induce a phase change. Instead, Li_3BN_2 crystallized directly in the monoclinic structure after the formation of the intermediate phase. Taking into account that $LiNH_2$ was observed in the fully decomposed state, the complete decomposition into imide Li_2NH was not observed. Similarly, Pinkerton *et al.*[17] did not find evidence about the presence of imide during dehydrogenation of catalysed $Li_4(NH_2)_3BH_4$, instead, they proposed the formation of a cubic phase containing Li–N–Cl–H due to the metal chloride additive. In our case, a non-stoichiometric phase with less hydrogen content than that of the amide was expected:

$$Li_3BN_2H_2 + LiNH_2 \rightarrow Li_3BN_2 + yNH_3 + H_2 + (1-y)Li_{1+x}NH_{2-x} \quad (13)$$

$$\text{In all: } Li_4(NH_2)_3BH_4 \rightarrow Li_3BN_2 + yNH_3 + 4H_2 + (1-y)Li_{1+x}NH_{2-x} \quad (14)$$

where $(1 + x) = 1/(1 - y)$. The second stage is characterized by NH_3 emission as the temperature increases, with additional H_2 production. Reaction (13) justifies an additional 2.2 wt% hydrogen while the remnant mass change measured by TG (Fig. 1) could be associated with NH_3 emission (about 0.4 mol%). The complete process takes into account that the amount of lithium amide gradually decreases.

As there is no LiH available, the interaction of the additive NiO in the $Li_4(NH_2)_3BH_4$–NiO sample differs from the $Li_4(NH_2)_3BH_4$–LiH–NiO sample despite the fact that in both cases metallic nickel was found in the decomposed state. To investigate the nature of the reaction between NiO and $LiNH_2$ or $LiBH_4$, additional measurements were performed with the $LiNH_2$–5 wt% NiO and $LiBH_4$–5 wt% NiO samples (Fig. S7, ESI†). The TG curves in Fig. S6 (ESI†) show that the interaction between NiO and $LiNH_2$ or $LiBH_4$ started at low temperature. The $LiNH_2$–NiO (5 wt%) sample displays a mass loss, reaching 3 wt% at 220 °C. This behavior shows a significant difference from that of $LiNH_2$ alone, which decomposes upon releasing NH_3 at higher temperatures. Instead, $LiBH_4$–NiO (5 wt%) presents a gradual and slow mass loss with increasing temperature. For reference, the direct reduction of NiO to Ni by hydrogen is shown and hydrogen release started at a high enough temperature (325 °C) to neglect its contribution. Taking into account this information, we propose that $LiNH_2$ and $LiBH_4$ interact with NiO during heating. The Ni particles could act as an active catalyst for direct $LiNH_2$ decomposition, producing N_2 and H_2 *via* a favorable path.[39,40] $Li_{1+x}NH_{2-x}$ formed during $LiNH_2$ decomposition can easily regenerate $LiNH_2$ in the vicinity of Ni. As it was previously suggested, Li creates a NH_x-rich environment and the Ni catalyst mediates the electron transfer facilitating NH_x coupling. In the case of $LiBH_4$, the release of H_2 is observed at low temperatures by breaking B–H bonds. Therefore, we can conclude that Ni particles play a relevant role in the decomposition of $Li_4(NH_2)_3BH_4$ but only when LiH is absent.

4. Conclusions

Due to the clear beneficial effects of $Li_4(NH_2)_3BH_4$ in the Li–N–B–H systems, we studied the influence of adding different oxides (5 wt% Co_3O_4 and 5 wt% NiO) to the $Li_4(NH_2)_3BH_4$–LiH composite to enhance its decomposition; reducing the operation temperature and formation of undesired gases (ammonia or diborane). Through this study we were able to clarify the effect of the different metal oxides and the role of LiH on the kinetics of the system and hence, the chemical interactions and the dehydrogenation reaction pathways.

The oxide additive had a clear destabilizing effect. For the doped composite, the dehydrogenation onset temperature was lower than that of the pristine material *i.e.* 14 °C and 32 °C for the Co and Ni-catalysed samples, respectively. In both cases, the additives were reduced to metallic species and in fact, the *in situ* formed Co and Ni acted as catalysts by breaking the B–H bonds of the Li–B–N–H species and promoted dehydrogenation processes. Furthermore, it was demonstrated that there was a common mechanism between the LiH containing samples with LiH playing a critical role and that the absence of LiH as a reactant forced the system to follow another path.

For the $Li_4(NH_2)_3BH_4$–LiH–NiO composite, the decomposition occurred *via* $LiNH_2$ and Li_3BN_2 formation (detected after 1 wt% of dehydrogenation), through a reaction that evolved hydrogen near its melting point, with a theoretical capacity of 8.1 wt%. Moreover the formation of lithium imide from the lithium amide contributed with an extra 1.7 wt% hydrogen. The difference between calculations and TG results was attributed to the ammonia emission, and 0.06 mol% NH_3 formation provided evidence for strong reduction of NH_3 emission. The sample was

partially re-hydrogenated only due to the rehydrogenation of lithium imide: 1.5 wt% hydrogen was released in the second dehydrogenation (calculated theoretical value: ~1.65 wt%).

For the $Li_4(NH_2)_3BH_4$–NiO composite, ammonia release at low temperatures was detected, which could be a consequence of the accommodation of $LiNH_2$ into the α-phase during heating. Decompositions at higher temperatures generated additional emissions of H_2 and NH_3. As a distinguishable issue, at the early stages of dehydrogenation, an intermediate phase of composition $Li_3BN_2H_2$ was formed. Moreover, in the completely decomposed state, reduced amounts of $LiNH_2$ were observed simultaneously with monoclinic Li_3BN_2. Thus, a non-stoichiometric phase, with lower hydrogen content than that of amide, was expected. Finally, the interaction between NiO and $LiNH_2$ or $LiBH_4$ at low temperature was shown. We propose that $LiNH_2$ interacts with NiO during heating and that Li creates an NH_x-rich environment and the Ni catalyst mediates the electron transfer facilitating NH_x coupling.

Conflicts of interest

There are no conflicts to declare.

Acknowledgements

This study was partially supported by CONICET (National Council of Scientific and Technological Research), CNEA (National Commission of Atomic Energy), ANPCyT (PICT No. 1052), Instituto Balseiro (University of Cuyo) and Pacific Northwest National Laboratory is operated for United States Department of Energy (DOE) by Battelle Memorial Institute. We thank Dr Molly O'Hagan for technical assistance related to the NMR instrument. We thank the Materials Characterization Department (GIA-GAATEN-CAB-CNEA) for the SEM images.

Notes and references

1 G. Walker. *Solid-state Hydrogen storage: Materials and Chemistry*, Woodhead Publishing Limited, England, 2008.
2 *Materials Research Society (MRS)*, ed. E. C. E Rönnebro and E. H. Majzoub, Bulletin, 2013, vol. 38, p. 6.
3 A. Sudik, J. Yang, D. J. Siegel, C. Wolverton, R. O. Carter and A. R. Drews, *J. Phys. Chem. C*, 2009, **113**, 2004.
4 J. J. Hu, M. Fichtner and P. Chen, *Chem. Mater.*, 2008, **20**, 7089.
5 J. J. Hu, Y. F. Liu, G. T. Wu, Z. T. Xiong, Y. S. Chua and P. Chen, *Chem. Mater.*, 2008, **20**, 4398.
6 J. Hu, E. Weidner, M. Hoelzel and M. Fichtner, *Dalton Trans.*, 2010, **39**, 9100.
7 Y. Liu, *Dalton Trans.*, 2013, **42**, 3802.
8 A. Borgschulte, M. O. Jones, E. Callini, B. Probst, S. Kato, A. Zuttel, W. I. F. David and S. Orimo, *Energy Environ. Sci.*, 2012, **5**, 6823.
9 F. E. Pinkerton, M. S. Meyer, G. P. Meisner and M. P. Balogh, *J. Alloys Compd.*, 2007, **433**, 282.
10 H. Wu, W. Zhou, K. Wang, T. J. Udovic, J. J. Rush, T. Yildirim, L. A. Bendersky, A. F. Gross, S. L. Van Atta, J. J. Vajo, F. E. Pinkerton and M. S. Meyer, *Nanotechnology*, 2009, **20**, 204002.
11 X. Zheng, G. Wu, W. Li, Z. Xiong, T. He, J. Guo, H. Chenb and P. Chen, *Energy Environ. Sci.*, 2011, **4**, 3593.
12 W. Luo and E. Rönnebro, *J. Alloys Compd.*, 2005, **404–406**, 392.
13 A. Zuttel, P. Wegner and S. Rentsch, *J. Power Sources*, 2003, **118**, 1.
14 F. E. Pinkerton, G. P. Meisner, M. S. Meyer, M. P. Balogh and M. D. Kundrat, *J. Phys. Chem. B*, 2005, **109**, 6.
15 J. P. Singer, M. S. Meyer, R. M. Speer Jr., J. E. Fischer and F. E. Pinkerton, *J. Phys. Chem. C*, 2009, **113**, 18927.
16 G. Meisner, M. L. Scullin, M. P. Balogh, F. E. Pinkerton and M. S. Meyer, *J. Phys. Chem. B*, 2006, **110**, 4186.
17 F. E. Pinkerton and M. S. Meyer, *J. Phys. Chem. C*, 2009, **113**, 11172.
18 J. Yang, A. Sudik, D. J. Siegel, D. Halliday, A. Drews, R. O. Carter, C. Wolverton, G. J. Lewis, J. W. Sachtler and W. A. Low, *Angew. Chem., Int. Ed.*, 2008, **47**, 882.
19 H. J. Cao, G. T. Wu, Y. Zhang, Z. T. Xiong, J. S. Qiu and P. Chen, *J. Mater. Chem. A*, 2014, **2**, 15816.
20 G. Amica, F. Cova, P. Arneodo Larochette and F. C. Gennari, *Phys. Chem. Chem. Phys.*, 2016, **18**, 17997.
21 X. Zheng, Z. Xiong, Y. Lim, G. Wu, P. Chen and H. Chen, *J. Phys. Chem. C*, 2011, **115**, 8840.
22 Y. H. Hu and E. Ruckenstein, *J. Phys. Chem. A*, 2003, **107**, 9737.
23 Y. Zhang, Y. Liu, X. Zhang, Y. Li, M. Gao and H. Pan, *Dalton Trans.*, 2015, **44**, 14514.
24 Y. Zhang, Y. Liu, Y. Pang, M. Gao and H. Pan, *J. Mater. Chem. A*, 2014, **2**, 11155.
25 H. Li, Y. Yan, E. Akiba and S. Orimo, *Mater. Trans.*, 2014, **55**, 1134.
26 J. R. Hattrick-Simpers, J. E. Maslar, M. U. Niemann, C. Chiu, S. S. Srinivasan, E. K. Stefanakos and L. A. Bendersky, *Int. J. Hydrogen Energy*, 2010, **35**, 6323.
27 J. Zhang, P. Li, Q. Wan, F. Zhai, A. A. Volinsky and X. Qu, *RSC Adv.*, 2015, **5**, 81212.
28 Y. Zhang, Y. Liu, T. Liu, M. Gao and H. Pan, *Int. J. Hydrogen Energy*, 2013, **38**, 13318.
29 X. Liu, D. Peaslee, C. Z. Jost and E. H. Majzoub, *J. Phys. Chem. C*, 2010, **114**, 14036.
30 P. Ngene, M. H. W. Verkuijlen, Q. Zheng, J. Kragten, P. Ja, M. van Bentum, J. H. Bitter and P. E. de Jongh, *Faraday Discuss.*, 2011, **151**, 47.
31 W. S. Tang, G. Wu, T. Liu, T. S. Andrew, C. K. Yong, A. Xiong, A. T. S. Hora and P. Chen, *Dalton Trans.*, 2008, 2395.
32 B. Liu, Z. P. Li and S. Suda, *J. Alloys Compd.*, 2006, **415**, 288.
33 T. He, Z. Xiong, G. Wu, H. Chu, C. Wu, T. Zhang and P. Chen, *Chem. Mater.*, 2009, **21**, 2315.
34 P. A. Chater, PhD thesis, University of Birmingham – School of Chemistry College of Engineering and Physical Sciences, 2009.
35 A. Wolczyk, A. E. Pinatel, M. R. Chierotti, C. Nervi, R. Gobetto and M. Baricco, *Int. J. Hydrogen Energy*, 2016, **41**, 14475.

36 M. Worle, H. M. Zu Altenschildesche and R. Nesper, *J. Alloys Compd.*, 1998, **264**, 107.
37 Outokumpu HSC Chemistry for Windows, version 6.1, Outokumpu Research Oy, Finland, 2009.
38 H. Cao, J. Wang, Y. Chua, H. Wang, G. Wu, Z. Xiong, J. Qiu and P. Chen, *J. Phys. Chem.*, 2014, **118**, 2344.
39 J. Guo, Z. Chen, A. Wu, F. Chang, P. Wang, D. Hu, G. Wu, Z. Xiong and P. Yu, *Chem. Commun.*, 2015, **51**, 15161.
40 J. Guo, P. Wang, G. Wu, A. Wu, D. Hu, Z. Xiong, J. Wang, P. Yu, F. Chang, Z. Chen and P. Chen, *Angew. Chem., Int. Ed.*, 2015, **54**, 2950.

